Desalination and Water Treatment
www.deswater.com

doi: 10.1080/19443994.2013.817510

52 (2014) 5952–5964
September

Taylor & Francis
Taylor & Francis Group

Adsorption profiles of some heavy metal ions from aqueous waste solutions using sodium-doped zirconium titanoslicate

B. El-Gammal

Hot Laboratories Center, Atomic Energy Authority, P.O. 13759, Cairo, Egypt
Email: belalelgammal@hotmail.com

Received 3 January 2012; Accepted 27 May 2013

ABSTRACT

Adsorption profiles of Co^{2+}, Cu^{2+}, Ni^{2+}, and Cr^{6+} ions from aqueous waste solutions were studied on novel sodium-doped zirconium titanoslicate (SDZTS) that was topographically transient pH characterized by a step change in ionic strength of buffer solutions. Using XRD, FTIR, and DTA–TGA, SDZTS-I, II, and III with single orthorhombic phases of Umbite [$K_2(Zr_{0.8}Ti_{0.2})Si_3O_9 \times H_2O$], Penkvilksite [$(Ti_{0.9}Zr.1)Si_4Na_2O_{13}H_4$], and Umbite [$K_2(Zr_{0.86}Ti.14)Si_3O_{10}H$], with P 21 21 21 (19), P n c a (60), and P 21 21 21 (19) space groups, were recognized, respectively. According to the transient pH procedure, they could be classified as cation ion-exchange chromatographic supports; the order of strength is SDZTS-III > SDZTS-II > SDZTS-I. The duration of the pH transient was linearly proportional to the total ionic capacity and was used to estimate active binding capacity of the resin. The break-through capacities, BTCs, obtained during dynamic measurements through the column experiments were less than the recorded static ion-exchange capacities, SIECs. The BTCs recorded for Cu^{2+}, Co^{2+}, Ni^{2+}, and Cr^{6+} /SDZTSs were SDZTS-III (2.45, 2.76, 2.25, and 3.97 meq/g), SDZTS-II (2.23, 2.65, 1.95, and 3.85 meq/g), and SDZTS-I (2.11, 2.42, 1.86, and 2.97 meq/g). The STIECs for Cu^{2+}, Co^{2+}, Ni^{2+}, and Cr^{6+} were in the order of SDZTS-III (6.42, 6.45, 4.57, and 5.25 meq/g)> SDZTS-II (5.82, 5.25, 4.14, and 4.96 meq/g > SDZTS-I (4.93, 4.35, 3.96, and 5.92 meq/g), respectively. Kinetic approaches, including the Lagergren first-order kinetic model (LFOKM), pseudo second-order kinetic model (PSOKM), and Morris–Weber kinetic model (MWKM), were used. They indicated that particle and/or film diffusion is the rate-determining step for Co^{2+}, Ni^{2+}, and Cr^{6+}/SDZTS-III, while chemical reaction is the controlling step in case of Cu^2/SDZTS-III. Langmuir and Freundlich models were selected as basic models for studying the different isotherms. Freundlich approach is a better fit for Co^{2+}, Ni^{2+}, and Cr^{6+}/SDZTS-III, while Langmuir is more appropriate in case of Cu^{2+}/SDZTS-III.

Keywords: Adsorption profiles; Concentration; Equilibrium and initial pH; Zirconium titanosilicate and doping effects

1. Introduction

One of the significant adverse impacts of industrial revolution is the hurried and indiscriminate demolition of our flora and fauna. Unusual kinds of health problems are arising due to heavy metals' contamination in the food chain and drinking water.

The heavy metals are real, nonbiodegradable, and may proceed to increase on each successive level in the food chain. Anthropogenic activities and industrial growth are conscientious for increased levels of heavy metals. Some of the metals in minute amounts are actually necessary for humans, while others are carcinogenic or lethal. These metals/ions may affect the central nervous system (e.g. Mn, Hg, Pb, etc.), the kidneys or liver (e.g. Hg, Pb, Cd, Cu, etc.), or skin, bones, or teeth (Ni, Cd, Cu, Cr, etc.) [1].

Many surface assimilation and bioadsoprtion techniques [2] have been recently studied for the discharge of heavy metal ions from wastewater for recycling it at lower cost. The ion-exchange method has been one of the most encouraging, simple, and popularly used chromatographic techniques employed in the purification of water [3]. The ion exchangers remove the charged species comprising metal ions either by exchanging it with other mobile ions or by adsorbing it [4]. Amelioration in the properties of ion-exchange materials has always been a goal of the workers by modifying the natural, inorganic, and polymeric ion exchangers to obtain a material with desirable ion-exchange characteristics, stability, and reproducibility [5].

Thus, the stepwise task of our present work is to synthesize novel inorganic ion-exchange adsorbents based on the sodium-doped zirconium titanosilicate precipitation approach. The new materials should be tested toward a list of target cationic species, such as Co^{2+}, Cu^{2+}, Ni^{2+}, and Cr^{3+}, for drinking water treatment. The adsorption profiles, including characterizations of their structural and surface chemical properties via transition pH should be adopted. Finally, the possible mechanisms and sequence routes for the sorption process should be emphasized.

2. Materials and methods

2.1. Materials, chemicals and reagents

Unless otherwise stated, the chemicals used were of analytical grade, and therefore no further purification was required. Both liquid titanium(IV)chloride, (98%), $TiCl_4$, 189.68 g/mol, 1.728 g/cm^3 (20˚C), and zirconium(IV)oxychloride octahydrate powder, (>99.5%), $ZrOCl_2{\cdot}8H_2O$, 322.26752 g/mol, 1.91 g/cm^3 (20˚C), pH value ~1 (50 g/l, H_2O, 20˚C), were purchased from Merck Chemicals, Darmstadt, Germany. From ACROS, USA, tetraethylorthosilicate, $(C_2H_5O)_4$ Si 208.33 g/mol, 0.93 g/cm^3 (20˚C) was used. On the other hand, sodiumtrisilicate solution, (>97%), $Na_2O(SiO_2)_x{\cdot}xH_2O$, 122.06 g/mol, 1.35 g/cm^3 (20˚C), pH value ~11.0–11.5 (50 g/l, H_2O, 20˚C) was supplied by Sigma Aldrich, USA. Further chemicals and reagents used were of analytical grade. High purity water was used in preparing solutions unless otherwise stated. Working standard solutions were prepared immediately before use by stepwise dilution from (1,000 mg/L) stock solutions for the ICP–OES measurements, supplied by Merck.

Three sodium-doped zirconium (IV) titanosilicates with different molar ratios were synthesized under controlled conditions by gradual addition of tetraethylortosilicate, dissolved in equal volumes of bidistilled water and ethyl alcohol with vigorous stirring to zirconium oxychlorideoctahydarte and titanium tetrachloride solutions previously dissolved in concentrated hydrochloric acid. While the reaction mixtures were thoroughly stirred with a turbulent velocity, at room temperature (25˚C), disodium dioxido(oxo)silane (pH ~11) was added as a dopant and to increase the pH of the system. Finally, the pH of the system was adjusted to 9 by liquid ammonia to ensure complete precipitation of the reacting precursors, and the experimental conditions were optimized so that the molar ratios of Zr:Ti:Si:Na were set as 8:2:3:2, 1:9:3:2, and 7:2:6:2, respectively. The obtained precipitates were left in the parent liquor intended for overnight standing. The slurries were refined, screened, filtered, and washed with deionized water for several times until they chloride-free and the pH of the supernatant suspension had a constant value (5.1 ± 0.01 for the prepared sodium-doped zirconium titanoslicate (SDZTS)s. The precipitates were then again filtered using a centrifuge (10^4 rpm), dried at 50˚C for four days, and then ground and sieved to obtain different mesh sizes and stored at room temperature.

2.3. Characterization of adsorbents

The chemical stability of the exchangers was appraised in a number of mineral acids and organic solvents so that 20 mL of different concentrations from each leachant was decanted on 0.2 g of SDZTSs held in 50-mL beaker and kept for 48 h with continuous shaking at room temperature. The concentrations of the liberated zirconium, titanium, silicon, and sodium ions were analyzed by means of ICP.

Crystallographic arrangements inside the SDZTSs structures, namely their powder X-ray diffractions, were made using the Shimadzu X-ray diffractometer (XRD), model XD610, with a nickel filter and Cu K_α radiation (1.54) operating at 30 kV and 30 mA.

The caloric reactions of the prepared exchangers under constant pressure of N_2 atmosphere were investigated employing Shimadzu simultaneous DTA

and TGA-60H thermal detectors obtained from Shimadzu, Kyoto, Japan.

FTIR spectra were acquired using a FTIR spectrometer following KBr disc procedure using FTIR model MB 157, Canada, in the range 4,000–400 cm^{-1} with a resolution of 4 cm^{-1} and wave-number accuracy of 1 cm^{-1}.

X-ray fluorescence (XRF) was carried out using Phillips X-ray Fluorescence, model PW 2400 spectrometer, the Netherlands, by applying the pressed-disc technique. Zirconium(IV) oxide, tin(IV) oxide, vanadium(III) oxide, and potassium oxide (Merck products) were thoroughly ground together to obtain solid reference samples for calibration; the error in the calibration curve was ± 0.2.

Morphology of different monoliths was examined using SEM technique after sputtering the specimens with gold using JEOL-TSM-5400 instrument, Japan, intraconnected to an EDX system.

2.4. Static capacity measurements

The static capacities for different metal ions were determined by batch technique. 500 mg of separate SDZTS-I, -II, and -III in Na^+ and H^+ forms were shaken with 5-ml 0.001 mol/L metal ion solutions at different pH values at 30 °C for 24 h (sufficient to attain equilibrium). The initial pH of the solution was adjusted using 0.05-M HCl solution and 0.050-M NaOH solution. After equilibrium, the solution was filtered and the metal ions were determined using ICP. The total ionic capacities of ion exchange of Na-doped zirconium titanosilicates were measured according to mass conversion. The difference in mass of dry monolithic support before and after the chemical modification was determined and normalized on the initial monolith mass. Dividing the normalized mass difference with the molar mass of the modifier according to theoretical stoichiometry of the reaction, the amount of introduced groups per gram of monolith was obtained. This value was considered as a total ionic capacity.

2.5. Column operation

An *in situ* flow-through cell was designed in the laboratory to maximize experimental flexibility, allow precise solution-flow control, and decrease the scattering contribution of the experimental cell to the diffraction pattern. A powdered sample was placed at the center of a 5.5-cm polyimide tube. The powder was held in place by glass wool on both sides which was supported by smaller sections (2 cm in length) of polyimide tubes. Flangeless ferrules with built-in 0.5-μm frits capped the larger polyimide tube. Solution flow rates were controlled with a peristaltic pump to maintain a drip rate of 2 drops/min.

Active group type on ion-exchange chromatographic column was determined by measuring pH contours obtained during step changes between base and high ionic strength buffers. Firstly, the column was equilibrated with low ionic strength buffer (25 mM Tris–HCl, pH 7.4) until stable absorbance at 200 nm and stable pH of the inlet solution were reached. Next, an immediate step change to high ionic strength buffer (25 mM Tris–HCl with 1 M NaCl, pH 7.4) was performed. After equilibrium between the ion exchanger and the feed solution was accomplished, the step change back to low ionic strength buffer was carried out. The pH of the eluent was well thought out. The magnitude and duration of transient pH excursions were determined.

The breakthrough ionic capacity measurement, BTIC, was executed by using two buffer solutions that varied in ionic strength, but had the same pH. For anionic capacity measurements, phosphate buffers of different concentrations were used. The column was first equilibrated with a high-concentration solution until the pre-saturation absorbance at 200 nm and pH were procured. The mobile phase flowing through the column was then switched at once to the low-concentration solution of the same solute having the same pH in order to form the pH transient. For cationic capacity measurement, solutions of Tris–HCl_2 buffer with and without sodium chloride and the same pH were used. The column was first equilibrated with a low ionic strength solution until the absorbance at 200 nm and pH of the inlet solution were reached. The mobile phase was then immediately switched to the high ionic strength solution having the same pH 5. The experiment was completed when the absorbance and the pH of the effluent reached 6 at the column inlet. The time between switching the mobile phases and reaching 50% absorbance of the "breakthrough" was determined.

2.6. Analysis

Measurements of the concentrations of cobalt, copper, nickel, and chromium were performed with sequential coupled plasma spectrometry, ICPS-7500, Shimadzu. All the concentration measurements were carried out using a four-point calibration. Multi-element calibration standards were used for all elements.

3. Results and discussion

3.1. Characterization

The chemical deteriorations of SDZTS-I, II, and III specimens in different media are listed in Table 1. They are considerably resistant to organic solvents, including methanol, ethanol, benzene, and toluene. These solvents could not destroy the structures of the tested materials even in their pure state. In addition, bidistilled water and dilute mineral acids behaved like organic solvents, i.e. Na^+, Zr^{4+}, Ti^{4+}, or Si^{4+} concentrations were under the detection limit (UD). However, they partially decompose in inorganic acidic solutions with concentrations of $\geqslant$1 mol/L. By taking the measured concentrations of Zr and Ti as references for skeletal degradations of mentioned exchangers, it was found that SDZTS-II was the most stable one. This relative stability might be attributed to its rigid crystal structure as well as the differences in water of crystallization, as indicated by thermal analysis measurements. The maximum sustainability of the prepared exchangers was estimated by evaluation of the maximum zirconium concentrations leached. In 3 M HCl, HNO_3, and H_2SO_4, the recorded values were about (17.3, 9.4, and 24.6 mg/L), (6.2, 12, and 18.5 mg/L), and (26.9, 17.4, and 32.7 mg/L) for SDZTS-I, II, and III, respectively. These SDZTSs are more likely to be stable than some titanium and zirconium vanadates, and even their potassium-doped exchangers [6,7]. The amounts of V^{4+} , leached out in 2 M HCl, 4 M HCl, 2 M HNO_3, 4 M HNO_3, 2 M H_2SO_4, 4 M H_2SO_4, 0.1 M NaOH, 1 M NaOH, ethanol, and benzene solution from the zirconium vanadate matrix, rather than bidistilled water, was about 4, 9, 2.2, 5.3, 4.1, 10.7, 6.4, 10.4, 0.0, and 0.0 Wt-%, respectively [7]. In an agreement, potassium zinc hexacyanoferrate(II) was found to be stable in water, dilute mineral acids, ethanol, methanol, acetone, and ether but it is soluble in concentrated mineral acids and 4 M NaOH solution [8].

Figs. 1–3 are the XRD patterns in different crystallographic planes, showing strong intensities for different exchangers, suggesting that the prepared materials are crystalline in nature at the ambient temperature. The data were obtained for both d-I and 2 theta-I at 1.54 . The data was subjected to complete analysis using Rietveld refinement by means of CMPR software after superposition of the peaks and fitting the data, as well as after background correction. It was found according to the Joint Committee on Powder Diffraction Standards, American Mineralogist Crystal Structure Database, and the International Centre for Diffraction Data that each XRD pattern was composed of a single phase. For SDZTS-I, II, and III, single orthorhombic phases of umbite [$K_2(Zr_{0.8}Ti_{0.2})$

Table 1
Chemical stabilities of TPV and ZPV ion exchangers in different media

HCl				HNO_3			H_2SO_4		
Concentration	SDZTS-I	SDZTS-II	SDZTS-III	SDZTS-I	SDZTS-II	SDZTS-III	SDZTS-I	SDZTS-II	SDZTS-III
0.01 M	UD	UD	UD	UD	UD	UD	UD	UD	UD
0.05 M	UD	UD	UD	UD	UD	UD	UD	UD	UD
0.1 M	UD	UD	UD	UD	UD	UD	UD	UD	UD
0.5 M	UD	UD	UD	UD	UD	UD	UD	UD	UD
1 M	UD	UD	5.2 ppm	UD	UD	7.3 ppm	UD	UD	11.1 ppm
2 M	2.7 ppm	2.1 ppm	8.1 ppm	13.6 ppm	9.3 ppm	11.2 ppm	15.6 ppm	11.6 ppm	13.5 ppm
3 M	17.3 ppm	9.4 ppm	24.6 ppm	16.2 ppm	12 ppm	18.5 ppm	26.9 ppm	17.4 ppm	32.7 ppm

UD: under detection.

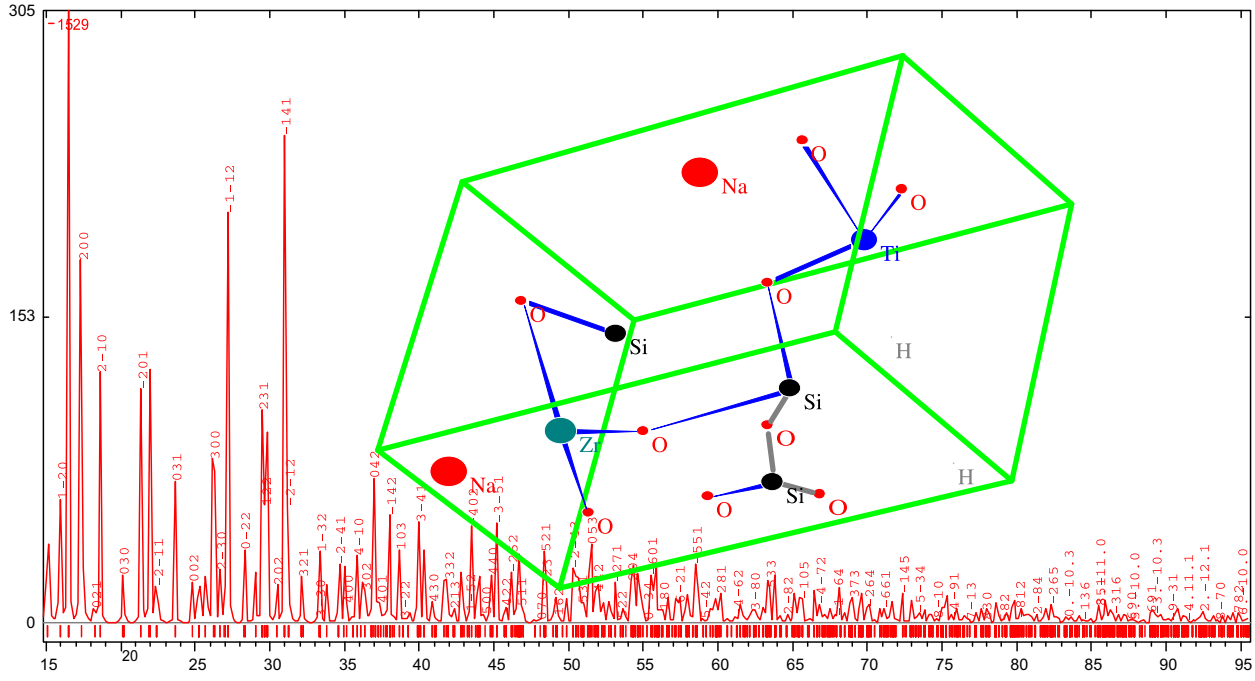

Fig. 1. XRD pattern and proposed unit cell of Umbite [$Zr_8Ti_2Si_3Na_2O_{12}H_6$].

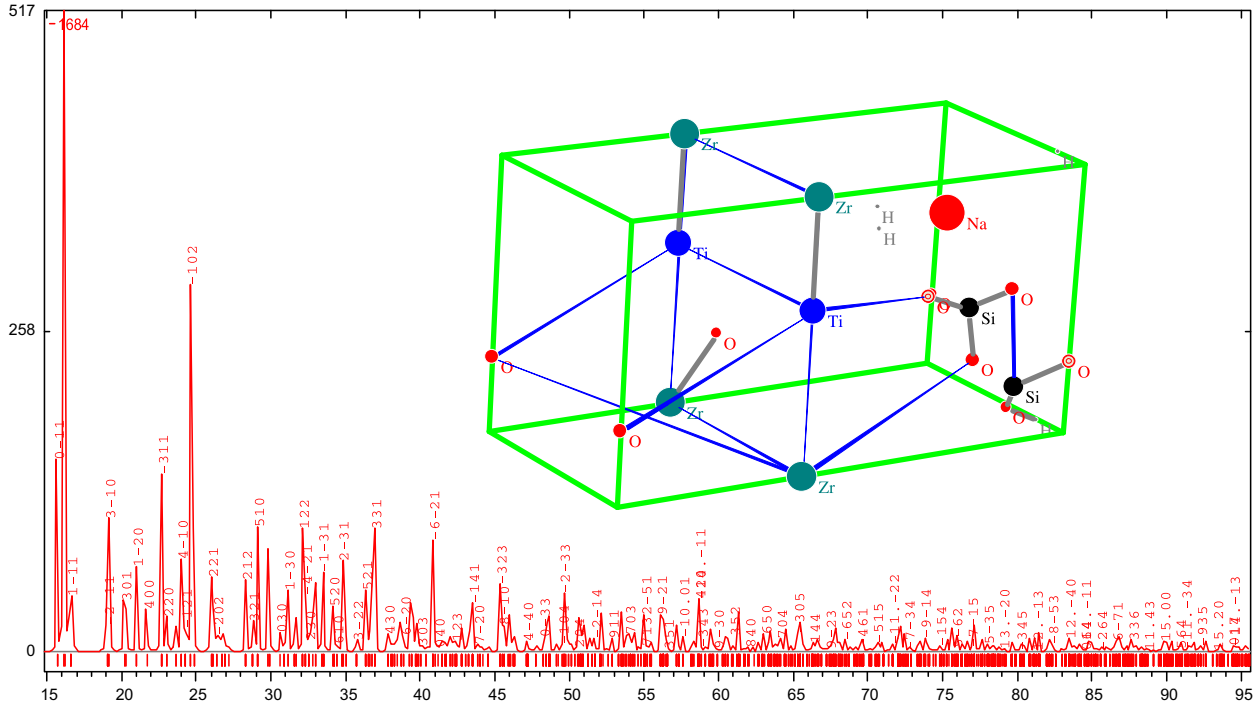

Fig. 2. XRD pattern and proposed unit cell of Penkvilksite [$ZrTi_9Si_{2.89}Na_{2.1}O_{13}H_4$].

$Si_3O_9{\cdot}H_2O$], Penkvilksite [$(Ti_{0.9}Zr.1)Si_4Na_2O_{13}H_4$], and umbite [$K_2(Zr_{0.86}Ti.14)Si_3O_{10}H$], with P 21 21 21 (19), P n c a (60), and P 21 21 21 (19) space groups, respectively [9–12]. The differences between the three phases are completely listed in Tables 2–5. Since, the pattern of heated umbite (500˚C) is virtually identical

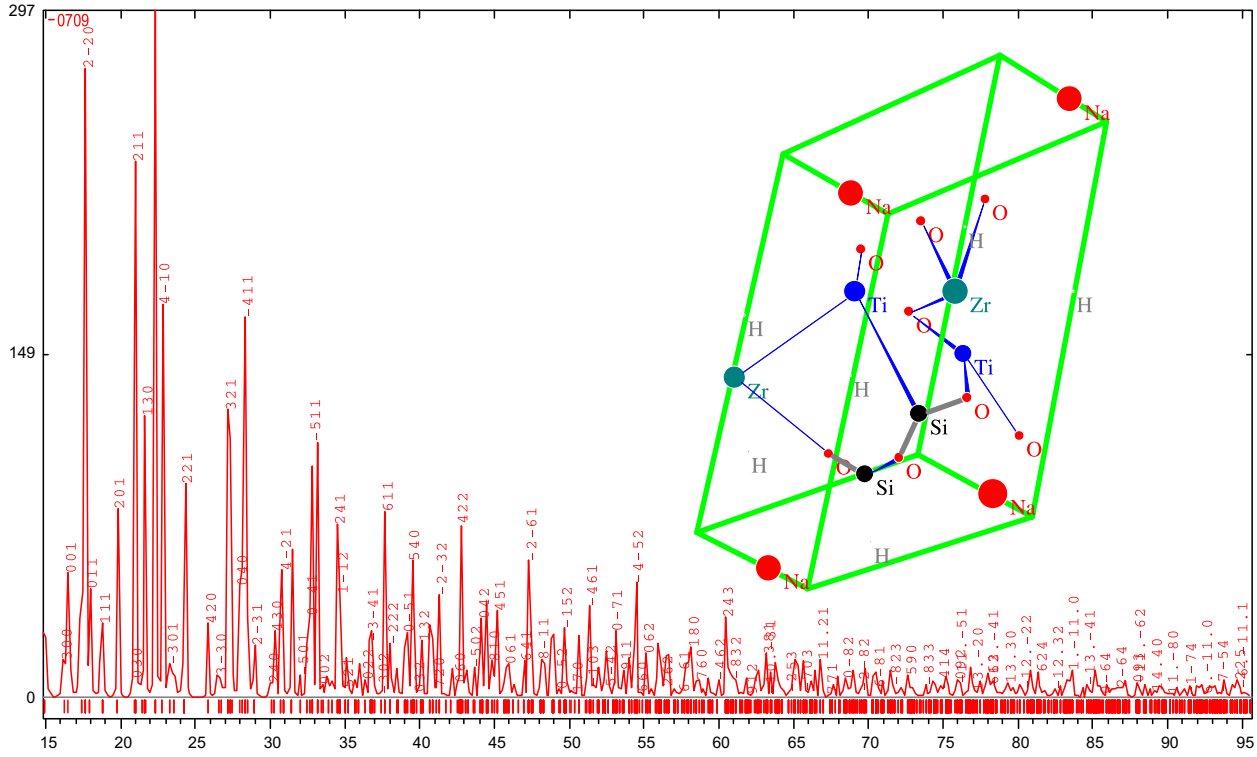

Fig. 3. XRD pattern and proposed unit cell of second Umbite [$Zr_7Ti_2Si_{6.1}Na_2O_{18}H_{18}$].

to that of Wadeite, dimorphous with Kostylevite, DTA is indispensible to distinguish between the different phases, especially between the two umbites. As can be seen in Table 5, the proposed formulae of SDZTS-I, II, and III were recorded as $Zr_8Ti_2Si_3Na_2O_{12}H_6$, $ZrTi_9Si_{2.89}Na_{2.1}O_{13}H_4$, and $Zr_7Ti_2Si_{6.1}Na_2O_{18}H_{18}$, respectively.

As indicated in Tables 2–4, the atom positions in 3D are in accordance with those shown in Figs. 1–3. However, the SOFs and thermal factors approximate to unity, except for Zr and Ti in SDZTs-I which have SOF values of 0.8500 and 0.1400, respectively. The titanium atoms are octahedrally coordinated and are located on a diagonal mirror plane and close to the 4_2 axis in the crystal. Thus, the symmetry generates a cluster of titanium, silicon, and zirconium atoms bridged together by O_2 atoms (average Ti–Zr = 3.1) that also lie on the mirror plane. Ti clusters are bridged by O_4 atoms along the *c* axis, while along *a* and *b* directions they are connected by Ti–O–Si–O–Zr–O–Ti linkages. However, direct M–M bonds are noticed, especially in SDZTS-II and III.

Table 5 shows the chemical constitutions and physical properties of different exchangers. The chemical analysis observed by both XRF and SEM–EDX agrees with the different molar ratios previously set

Table 2
Positional and thermal parameters for SDZTS-I

Element		Atom coordinates			Thermal factors	
Symbol	*Z*	*X*	*Y*	*Z*	SOF	*B*
Na	11	−0.03150	0.54780	0.73550	1.0000	1.0000
Na	11	0.00450	0.93480	0.77350	1.0000	1.0000
Zr	40	0.04550	0.67980	0.78350	0.8500	1.0000
Ti	22	−1.06450	0.37980	0.18350	0.1400	1.0000
Si	14	0.17150	0.29780	0.52850	1.0000	1.0000
Si	14	−0.36650	0.80280	0.44140	1.0000	1.0000
Si	14	0.02850	0.42180	0.25340	1.0000	1.0000
O	8	0.16350	0.65780	0.06550	1.0000	1.0000
O	8	0.78150	0.53380	0.29250	1.0000	1.0000
O	8	0.20450	0.65680	0.45750	1.0000	1.0000
O	8	−0.09150	0.19980	0.43240	1.0000	1.0000
O	8	−0.34750	0.91080	−1.27650	1.0000	1.0000
O	8	0.07450	0.83580	0.26840	1.0000	1.0000
O	8	−0.00450	0.32480	0.72350	1.0000	1.0000
O	8	0.15150	0.39580	0.39650	1.0000	1.0000
O	8	0.09050	0.40780	0.04140	1.0000	1.0000
H	1	0.17650	0.03480	0.65140	1.0000	1.0000
H	1	0.09550	0.12580	0.02350	1.0000	1.0000

Table 3
Positional and thermal parameters for SDZTS-II

Element		Atom coordinates			Thermal factors	
Symbol	Z	X	Y	Z	SOF	B
Ti	22	−0.4000	−0.40000	0.00000	1.0000	1.0000
Zr	40	0.60000	0.00000	1.00000	1.0000	1.0000
Si	14	0.08300	0.16100	0.12500	1.0000	1.0000
Si	14	0.15700	0.44000	0.26000	1.0000	1.0000
Na	11	0.10200	0.69100	0.62200	1.0000	1.0000
O	8	0.16000	0.26100	0.20100	1.0000	1.0000
O	8	0.05000	0.03700	0.27000	1.0000	1.0000
O	8	−1.00000	0.27000	1.00000	1.0000	1.0000
O	8	0.51600	0.25100	0.96100	1.0000	1.0000
O	8	0.11200	0.53900	0.10500	1.0000	1.0000
O	8	−0.75000	0.50000	0.27100	1.0000	1.0000
H	1	0.19500	0.68400	−0.15500	1.0000	1.0000
H	1	0.17300	0.58600	−0.10800	1.0000	1.0000
H	1	0.00000	0.00000	0.19500	1.0000	1.0000

Table 4
Positional and thermal parameters for SDZTS-III

Element		Atom coordinates			Thermal factors	
Symbol	Z	X	Y	Z	SOF	B
Ti	22	−0.50000	0.46330	0.00000	1.0000	1.0000
Zr	40	−0.40000	0.00000	0.03450	1.0000	1.0000
Si	14	−0.14710	0.12430	0.15950	1.0000	1.0000
Si	14	−0.07310	0.40330	0.29450	1.0000	1.0000
Na	11	0.00000	0.00000	0.65650	1.0000	1.0000
O	8	−0.07010	0.22430	0.23550	1.0000	1.0000
O	8	−0.18010	0.00030	0.30450	1.0000	1.0000
O	8	0.36990	0.23330	0.03450	1.0000	1.0000
O	8	0.78590	0.11430	−1.00450	1.0000	1.0000
O	8	−0.11810	0.50230	0.13950	1.0000	1.0000
O	8	0.30000	0.10000	−1.69450	1.0000	1.0000
O	8	0.24330	0.76550	0.46360	1.0000	1.0000
O	8	0.42340	0.56760	0.64650	1.0000	1.0000
H	1	−0.03510	0.64730	−0.12050	1.0000	1.0000
H	1	0.44290	0.00000	0.00000	1.0000	1.0000
H	1	−0.23010	0.96330	0.22950	1.0000	1.0000

during the preparation process. Different types of water are recorded based on both the FTIR analysis and DTA procedures. The FTIR results indicated the presence of water molecules, as mentioned by the presence of broad peaks at about 3,200 cm^{-1} against different peaks below 950 cm^{-1} due to M–O and M–M stretching modes. Analysis of the water peaks revealed that the total water inside different exchangers is about 7.6, 8.82, and 14.89 for SDZTS-I, II, and III, respectively. Deeper investigation and differentiation will be later discussed in the ion-exchange sections.

3.2. Adsorption profiles

3.2.1. Determination of ion-exchange active group type

The ion-exchange active group types were achieved by applying the transient pH phenomenon. Figs. 4–6 determine these profiles according to the buffer used. As seen in the figures, the buffer systems for common ion-exchange chromatographic applications, as used for purification or separation of samples, having charged macromolecules should have a high buffer capacity to prevent extreme pH changes in the chromatographical system during the run. In our system, buffering ions have the same charge species as the ion exchanger; otherwise, the buffering species bind to the surface and take part in the ion-exchange process. This can lower the capacity of the resin for the target molecule and cause significant pH fluctuations during the elution step, which can affect the chromatographic process. Furthermore, buffer p*Ka* values are within 0.65 pH units of the working pH to gain sufficient buffering capacity [13].

It can be observed that after the step change from Tris–HCl buffer to Tris–HCl buffer with sodium chloride, the effluent pH for cation-exchange columns drops for more than 1 pH unit.

Only in Fig. 6 the elution volume of the transient pH change caused by the step change from low to high ionic strength buffer is smaller, as it is in the case of the reversed step. On the other hand, for SDZTSs-I and II, the elution volumes of the transient pH are inversed; after the first step, the volume is larger than after the second step, as indicated in Figs. 4 and 5.

The pH excursions are quite sensitive to the buffer conditions, such as pH and concentration. Thus, to make the characterization method sensitive and robust enough, this should be examined and the final conditions should be determined according to the experiments. When using weak ion exchangers, significant pH change during the elution process might occur even if the buffering species have the same charge as the functional groups of the ion exchanger and pH of the mobile phase is near buffer's p*Ka* [14–17]. In this manner, the order of strength is:t

SDZTS-III > SDZTS-II > SDZTS-I

3.2.2. Static ion-exchange capacities

After the pH transition phase's characterizations, the ion-exchange capacities, IECs, of SDZTS-I, II, and

Table 5
Chemical analysis and physical properties of different exchangers

		SDZTS-I	SDZTS-II	SDZTS-III
Chemical analysis	Na	3.64	5.15	3.66
	Si	6.68	12.59	13.43
	O	22.82	23.30	22.95
	Zr	57.83	10.22	50.88
	Ti	7.59	48.29	7.63
	H	1.44	0.45	1.45
Cell parameters, A°	*a*	10.208	16.372	16.33
	b	13.241	8.749	12.74
	c	7.174	7.402	5.35
Theoretical cell volume, A^{o3}		965.42	1060.25	1113.23
Measured cell volume, A^{o3}		969.66	1064.84	1116.92
Calculated density, g/cm^3		3.942	2.68	2.81
Measured density, g/cm^3		3.22	2.69	2.89
Color		Pale yellow	Yellow	Greenish yellow
Molecular weight		1153.85	892.68	1261.94
Water differentiation	External	3.13	4.95	3.52
	Loosely bound	2.17	2.27	5.66
	Tightly bound	2.3	1.6	5.71
	L/T ratio	0.9431	1.4187	0.9912
	Exchanging water	4.47	3.87	11.37
	Total water	7.6	8.82	14.89
Proposed formula		$Zr_8Ti_2Si_3Na_2O_{12}H_6$	$ZrTi_9Si_{2.89}Na_{2.1}O_{13}H_4$	$Zr_7Ti_2Si_{6.1}Na_2O_{18}H_{18}$

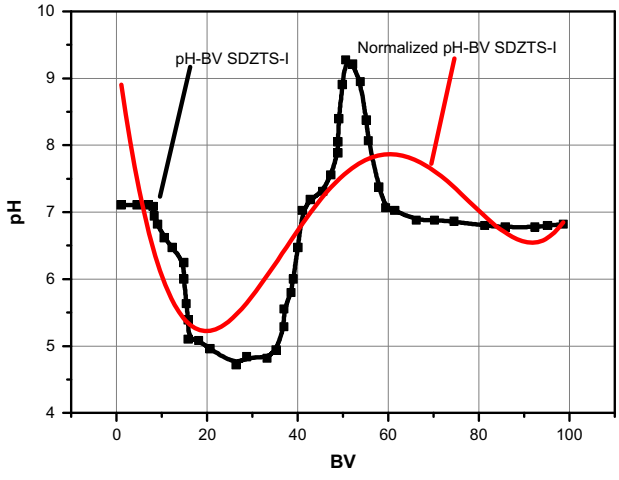

Fig. 4. Transient pH elution curves for SDZTS-I column.

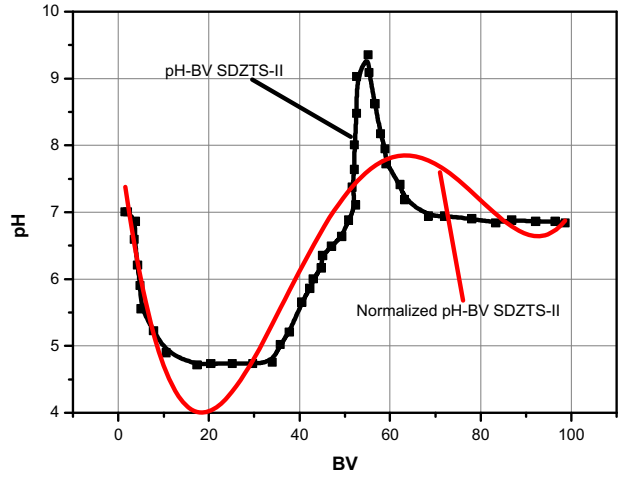

Fig. 5. Transient pH elution curves for SDZTS-II column.

III were evaluated at pH 4 in both the static and dynamic modes after soaking the exchanger in the aforementioned cations solutions and passing these solutions through bed columns, respectively, in order to ratiocinate the doping effect of Na into the structure of the exchange resins. The amount of metal ion sorbed, *q*, per gram of sorbent was estimated using the equation:

$$q = (C_i - C) \times \frac{V}{m} \quad (1)$$

where C_i and C are the initial and final concentrations in milligram per liter in the solution, respectively, V is the initial volume of the metal ion solution in mL, and m is the dry mass of the exchanger in g.

Static ion-exchange capacities (SIEC)s for Cu^{2+}, Co^{2+}, Ni^{2+}, and Cr^{6+} / bare zirconium silicate surface

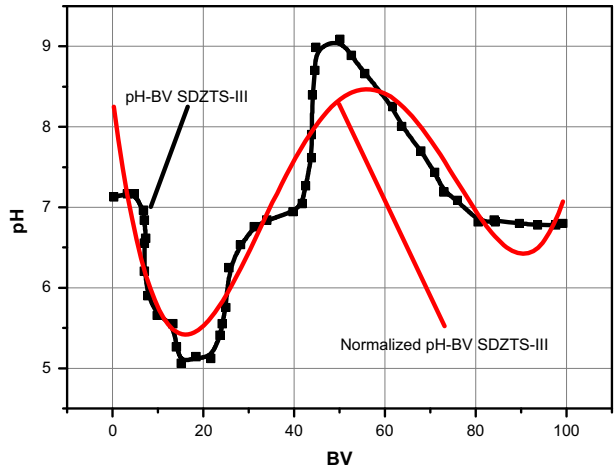

Fig. 6. Transient pH elution curves for SDZTS-III.

were about (1.75, 1.87, 184, and 1.99 meq/g). These values were in the same trend but in less order than the constructed SIECs for the same cations Cu^{2+}, Co^{2+}, Ni^{2+}, and Cr^{6+} that were about (2.81, 2.89, 2.73, and 2.97 meq/g) and (2.18, 1.98, 2.16, and 3.61 meq/g) on TPV and ZPV surfaces, respectively, that were enhanced by doping the exchanger with potassium in certain ratio [7].

By using Na^{+} as a dopant, the SIECs for the studied ions were markedly raised to about two orders of magnitude of the original values, according to the preparation conditions of the exchangers. As indicated from the XRD–DTA measurements, the SIECs are in accordance with the total water trapped in the pores of the exchangers. As a result, the STIEC for Cu^{2+}, Co^{2+}, Ni^{2+}, and Cr^{6+} were in the order of SDZTS-III (6.42, 6.45, 4.57, and 5.25 meq/g) > SDZTS-II (5.82, 5.25, 4.14, and 4.96 meq/g > SDZTS-I (4.93, 4.35, 3.96, and 5.92 meq/g), respectively. These values were comparable to those found in some exchange systems, including zirconium oxide, and/or silicon oxide in their skeleton.

When zirconium iodotungstate, ZIW, was set as new exchanger [18], its SIEC toward some alkaline earth ions, transition metal ions, and lanthanide ions was indicated. The values of the SIEC retained by ZIW were less than those reported in the current SDZTSs I, II, and III, except for Ba^{2+}, Bi^{2+}, and Co^{2+}. The recorded IECs were 0.9, 0.71, 1.34, 4.60, 0.56, 1.78, 1.36, 0.27, 0.24, 8.78, 8.73, 0.68, 2.09, 3.26, 7.47, 2.88, and 0.63 meq of Mg^{2+}, Ca^{2+}, Sr^{2+}, Ba^{2+}, Zn^{2+}, Cd^{2+}, Cu^{2+}, Ni^{2+}, Pb^{2+}, Al^{3+}, Hg^{2+}, Bi^{3+}, Co^{2+}, Fe^{3+}, Zr^{4+}, Th^{4+}, La^{3+}, and Mn^{2+} per one g of ZIW, respectively.

The SIECs of zirconium(IV) tungestoiodophosphate (ZTIP) toward Li^{+}, Na^{+}, K^{+}, Mg^{2+}, Sr^{2+}, and Ca^{2+} were about 1.9, 2.2, 2.35, 1.45, 1.68, and 1.85 meq/g, respectively [19]. Accordingly, tin (IV) tungstovanadophosphate (TTVP), zirconium(IV) iodophosphate (ZIP), and zirconium(IV) iodomolybdate (ZIM) indicated that the IECs of ZTIP, TTVP, ZIP, and ZIM toward Na^{+} ions decreased with increase in calcination temperature. The obtained IECs for ZTIP were about (2.2, 1.85, 1.60, 1.35, 1.0, 0.90, and 0.78 meq/g), (1.83, 1.80, 1.50, 1.25, 0.97, 0.85, and –meq/g), (1.75, 1.60, 1.40, 1.0, 0.92, 0.82, and 0.66 meq/g), (1.54, 1.30, 1.0, 0.78, 0.66, 0.42, and 0.16 meq/g) on heating the exchangers at 40, 100, 200, 300, 400, 500, and 600˚C, respectively.

On the other hand, the breakthrough capacities, BTCs, obtained during dynamic measurements through the column experiments were less than the recorded SIECs. The BTCs recorded for Cu^{2+}, Co^{2+}, Ni^{2+}, and Cr^{6+} /SDZTSs were SDZTS-III (2.45, 2.76, 2.25, and 3.97 meq/g), SDZTS-II (2.23, 2.65, 1.95, and 3.85 meq/g), and SDZTS-I (2.11, 2.42, 1.86, and 2.97 meq/g). These values are in accordance with the total and differential water contents registered in Table 5.

3.2.3. Kinetic profiles

Fig. 7 illustrates the adsorption of Cu^{2+}, Co^{2+}, Ni^{2+}, and Cr^{6+} /SDZTS-III. The amount of heavy metal ion uptake, q_t, meq g^{-1}, increased with increase in contact time. The ion uptake was rapid within the first 2.5 h, and then proceeded at a slower rate until it finally reached equilibrium within 5 h.

The behavior of the heavy metal ion adsorption was analyzed using the LFOKM, the PSOKM, and the MWKM [20,21]. The linear form of LFOKM could be written as:

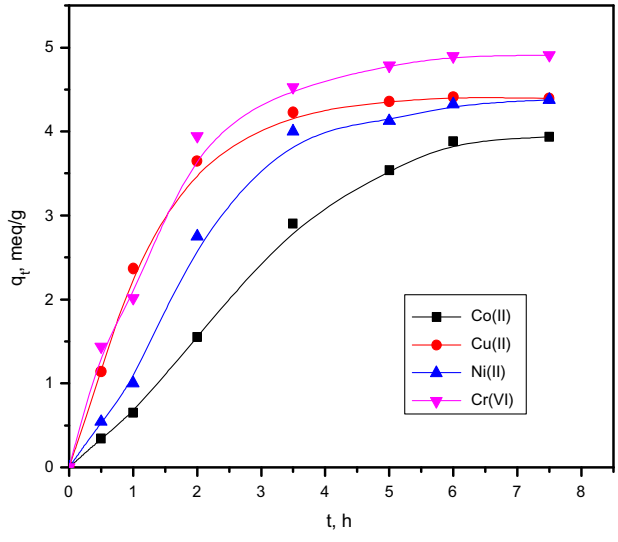

Fig. 7. Time q_t kinetic profiles of Cu^{2+}, Co^{2+}, Ni^{2+}, and Cr^{6+} on SDZTS-III.

Table 6
LFOKM and PSOKM rate constants of Cu^{2+}, Co^{2+}, Ni^{2+}, and Cr^{6+} /SDZTS-III

Adsorbate	q_e/meq g^{-1}	LFOKM			PSOKM		
		k_1/min^{-1}	$q_{e.c}$/mg g^{-1}	R^2	k_2/g mg^{-1} min^{-1}	$q_{e.c}$/meg g^{-1}	R^2
Co^{2+}	3.16	1.18	11.61	0.669	0.05	2.15	0.845
Cu^{2+}	4.34	0.83	5.21	0.586	6.45	2.09	0.986
Ni^{6+}	3.53	0.74	7.38	0.768	0.57	0.37	0.856
Cr^{6+}	4.39	0.94	8.35	0.766	9.45	1.09	0.698

$$\log(q_e - q_t) = \log q_e - \frac{k_1}{2.303}t \quad (2)$$

where q_e and q_t (mg g^{-1}) are the amount of heavy metal ions adsorbed at equilibrium and time t (min), respectively, and k_1 (min^{-1}) is the rate constant of the LFOKM (min^{-1}).

The kinetic data were further analyzed using the PSOKM, described by the following equation:

$$\frac{t}{q_t} = \frac{1}{k_2 q_e^2} + \frac{1}{q_e}t \quad (3)$$

where k_2 (g mg^{-1} min^{-1}) is the rate constant of pseudo-second-order adsorption. The validity of the data to PSOKM would be led to $t/q_t - t$ linear relationships.

The term $q_{e,c}$ is the amount of adsorption calculated from Eqs. (2) and (3). Values for $q_{e,c}$, k_1, and k_2 and the corresponding linear regression correlation coefficient R^2 values are shown in Table 6. The regression correlation coefficients of the LFOKM for Cu^{2+}, Co^{2+}, Ni^{2+}, and Cr^{6+}/SDZTS-III are very weak, while they are slightly acceptable for Cu^{2+}, Co^{2+}/SDZTS-III using PSOKM. These values agreed with the calculated and experimental loading capacities as shown in Table 6.

Since neither the LFOKM nor PSOKM were considered as weak models for the adsorption of Cu^{2+}, Co^{2+}, Ni^{2+}, and Cr^{6+}/SDZTS-III, and includes no diffusion mechanism, an intraparticle diffusion model was also used to evaluate the data and elucidate a diffusion mechanism. Transport from the bulk solution into the solid phase with an intraparticle diffusion process is often the rate-limiting step in many adsorption processes [20]. The possibility of intraparticle diffusion was explored by using the intraparticle diffusion model as described by Eq. (4):

$$q_t = k_{id}t^{1/2} + C \quad (4)$$

where C is the intercept and k_{id} is the intraparticle diffusion rate constant. Plots of q_t vs. $t^{1/2}$ for the adsorption of Cu^{2+}, Co^{2+}, Ni^{2+}, and Cr^{6+}/SDZTS-III are shown in Fig. 8. The values k_{id} and C, and the corresponding R^2 are given in Table 7. As seen from Fig. 8, the diffusion model of Co^{2+}, Cu^{2+}, Ni^{2+}, and Cr^{6+}/SDZTS-III includes both intraparticle diffusion and film diffusion. On the other hand, a clear investigation of Table 7 showed that the intercept of the same ions was 0.2505, −0.736, 0.7601, and −1.17302, leading to an approximation that the adsorption of Co^{2+}/SDZTS-III is merely a particle diffusion mechanism.

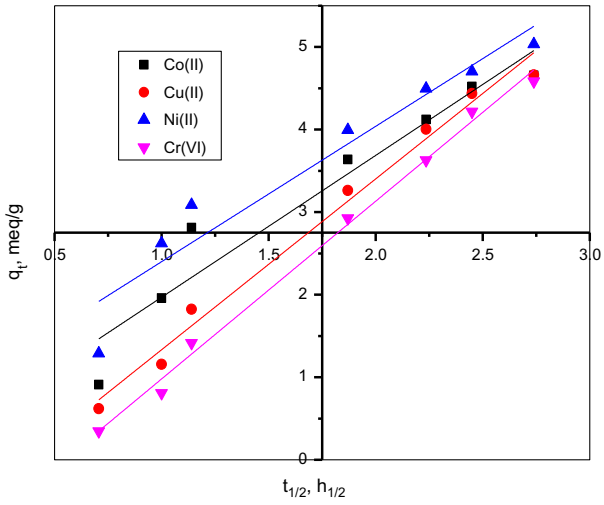

Fig. 8. Morris-Weber kinetic profiles of Cu^{2+}, Co^{2+}, Ni^{2+}, and Cr^{6+} on SDZTS-III.

Table 7
MWKM rate constants of Cu^{2+}, Co^{2+}, Ni^{2+}, and Cr^{6+}/SDZTS-III

Adsorbate	k_{id}/mg g^{-1} min$^{-1/2}$	C	R^2
Co^{2+}	3.36	0.2505	0.919
Cu^{2+}	4.75	−0.736	0.985
Ni^{2+}	3.21	0.7601	0.917
Cr^{6+}	5.46	−1.17302	0.994

The determined k_{id} values for Co^{2+}, Cu^{2+}, Ni^{2+}, and Cr^{6+}/SDZTS-III were about 3.36, 4.75, 3.21, and 5.46 mg g^{-1} $min^{-1/2}$, respectively. The determined R^2 asset value for the same ions was about 0.9192, 0.98457, 0.91729, and 0.99403.

As indicated in Tables 6 and 7, in comparison with the R^2 of both PSOKM and MWKM chemical reactions, clearly the sorption of Cu^{2+}/SDZTS-III could switch between the chemical reaction mechanism and the particle diffusion route.

3.2.4. Isothermal profiles

Fig. 9 illustrates the adsorption isotherm of Co^{2+}, Cu^{2+}, Ni^{2+}, and Cr^{6+}/SDZTS-III with different initial concentrations at 298 K. Langmuir and Freundlich isotherm models were used in their linear forms, Eqs. (5) and (6), to study the adsorption of these ions at equilibrium.

$$\frac{1}{q_e} = \frac{1}{Q^0} + \left(\frac{1}{bQ^0}\right)\left(\frac{1}{C_e}\right) \tag{5}$$

$$\log q_e = \log K_F + \frac{1}{n}\log C_e \tag{6}$$

where C_e is the equilibrium concentration of the solute (mg L^{-1}), Q^0 is the amount of solute adsorbed per unit mass of adsorbent in forming a complete monolayer on the surface (mg g^{-1}), b is a constant related to the affinity of binding sites (L mg^{-1}), and K_F (mg g^{-1}), and n are Frendlich constants related to adsorption capacity and adsorption intensity, respectively. The terms Q^0 and b were calculated from the slope and intercept of the straight-line plots of $1/q_e$ vs. $1/C_e$, and K_F and n are determined from the linear plot of log q_e vs. log C_e.

Fig. 10 represents the Freundlich adsorption isotherms for Co^{2+}, Cu^{2+}, Ni^{2+}, and Cr^{6+}/SDZTS-III; Langmuir and Freundlich constants are recorded in Table 8.

The regression correlation coefficients (R^2) of the Langmuir model for Co^{2+}, Cu^{2+}, Ni^{2+}, and Cr^{6+}/SDZTS-III were about 0.745, 0.935, 0.648, and 0.847, while the R^2 values of the Freundlich model were about 0.982, 0.901, 0.975, and 0.981 for the same ions on the same exchanger. These indicate strong correlations to the Freundlich adsorption model for all ions, except for Cu^{2+}/SDZTS-III, which is accurately fitted to the Langmuir model. As a measure of adsorption capacity of an adsorbent, and the strength of the relationship between the adsorbate and the adsorbent, the K_F was calculated and the results are indicated in Table 8. The K_F values of Co^{2+}, Cu^{2+}, Ni^{2+}, and Cr^{6+}/SDZTS-III were about 1.57, 1.89, 1.56, and 4.24 mg g^{-1}, respectively.

In all cases, the Freundlich exponent, n, is between 1 and 10, I. E., $(1 < n < 10)$, which is typically between 2.45 and 4.39 indicating favorable adsorption conditions.

The characteristics of Langmuir isotherm could be expressed in terms of a dimensionless constant separation factor, I. E, the equilibrium parameter, R_L, expressed by Eq. (7) as:

$$R_L = \frac{1}{1 + bC_0} \tag{7}$$

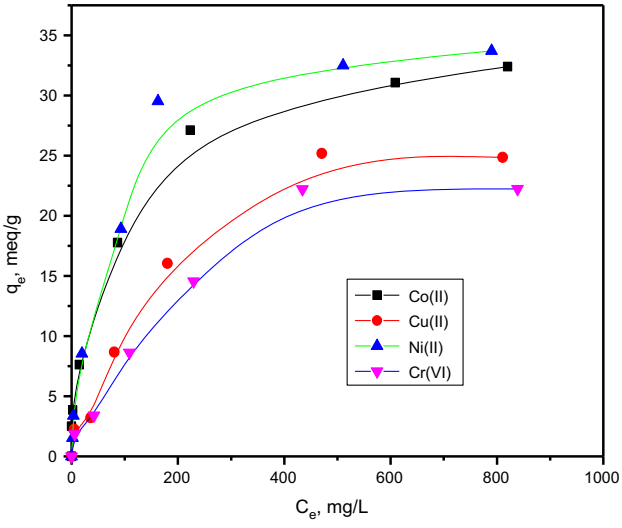

Fig. 9. $C_e - q_e$ Isothermal profiles of Cu^{2+}, Co^{2+}, Ni^{2+}, and Cr^{6+} on SDZTS-III.

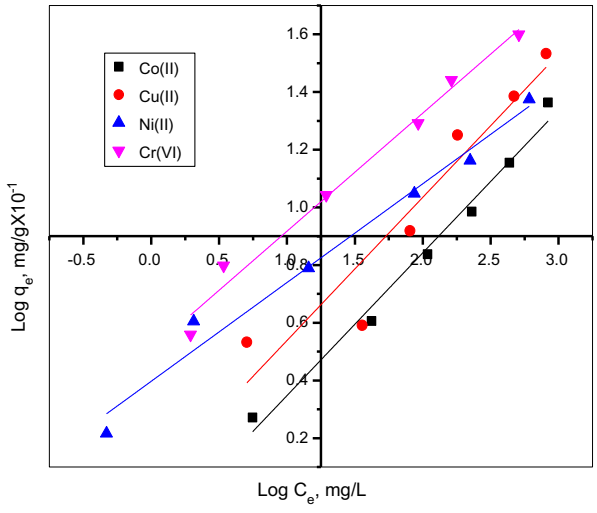

Fig. 10. Freundlich isothermal profiles of Cu^{2+}, Co^{2+}, Ni^{2+}, and Cr^{6+} on SDZTS-III.

Table 8
Langmuir and Freundlich constants for Co^{2+}, Cu^{2+}, Ni^{2+}, and Cr6+/SDZTS-III

Adsorbate	Langmuir constants				Freundlich constants		
	$Q^0/mg\,g^{-1}$	$b \times 10^2/L\,mg^{-1}$	R^2	R_L	$K_F/mg\,g^{-1}$	n	R^2
Co^{2+}	34.71	7.33	0.745	0.23	1.57	2.45	0.982
Cu^{2+}	87.97	37.58	0.935	0.16	1.89	3.43	0.901
Ni^{2+}	56.22	8.56	0.648	0.18	1.56	2.79	0.975
Cr^{6+}	127.13	6.50	0.847	0.36	4.24	4.39	0.981

where b is the Langmuir constant and C_0 is the initial concentration of heavy metal ions.

The R_L indicates the type of the isotherm as being either unfavorable ($R_L > 1$), linear ($R_L = 1$), suitable ($0 < R_L < 1$), or irreversible ($R_L < 0$) [22]. As shown in Table 8, the R_L values lie between 0.16 and 0.36, indicating an advantageous adsorption for all ions on SDZTS-III, which agrees with the results obtained for the adsorption of some azo dyes from aqueous phase on activated charcoal-based sorbents [23].

4. Conclusions

Three types of SDZTSs were prepared and characterized using different tools. Modern head-on analysis approach for the adsorption profiles of Co^{2+}, Cu^{2+}, Ni^{2+}, and Cr^{6+} on sodium-doped zirconium(IV) titanosilicate exchangers was adopted, depending upon the type of active groups. The strength of the groups was inspected based on transient pH created by a step change in ionic strength of buffers. The method could be used to distinguish between the enterprising groups on ion-exchange chromatographic columns of any kind. It was shown that the time span of pH transient is linearly proportional to the total ionic capacity, and once the method is calibrated it can be directly used to determine the ionic capacity of SDZTS' structures of columns of any size and shape. The method can be adjusted to the particular ion-exchange system by optimizing the buffer's type, pH, concentration, and temperature in case of weak ion exchangers. Since the application this method did not result in any contamination and does not damage the structure of the chromatographic resin, the method is very convenient for quality control of the produced ion-exchange chromatographic columns, notably massive columns and microporous membranes. Moreover, noninvasiveness and simplicity enable users of chromatographic columns to use the method for monitoring the chromatographic properties of columns during their storage and their use, especially to monitor the ligand degradation and surface structures even in mixed modes. Following to step, kinetic modeling was applied to determine the exact mechanisms of Co^{2+}, Cu^{2+}, Ni^{2+}, and Cr^{6+}/SDZTS-III. Three models, including LFOKM, PSOKM, and MWKM, were applied. The results indicated that the LFOKM is considered as the low-fit model for Co^{2+}, Cu^{2+}, Ni^{2+}, and Cr^{6+}/SDZTS-III. In case of PSOKM, the data are only fitted to Cu^{2+}/SDZTS-III, while the MWKM was applicable to Co^{2+}, Cu^{2+}, Ni^{2+}, and Cr^{6+}/SDZTS-III with high linear regression correlation coefficients. This data suggested that mixed particle and film diffusion mechanisms are predominant for Co^{2+}, Ni^{2+}, and Cr^{6+}/SDZTS-III, whereas switching between particle diffusion and chemical reaction could be seen in case Cu^{2+}/SDZTS-III. As a follow-up procedure, the isothermal profiles at 298 K were tested. Langmuir and Freundlich were used as basic isothermal models. Freundlich equation was typically fitted to the adsorption of Co^{2+}, Cu^{2+}, Ni^{2+}, and Cr^{6+}/SDZTS-III. However, a better fit of Cu^{2+}/SDZTS-III was seen, which confirms the chemical reaction between the cupric ions and SDZTS-III surface.

References

[1] Q. Yuan, N. Li, Y. Chi, W. Geng, W. Yan, Y. Zhao, X. Li, B. Dong, Effect of large pore size of multifunctional mesoporous microsphere on removal of heavy metal ions, J. Hazard. Mater. 254–255(15) (2013) 157–165.
[2] N. Wu, Z. Li, Synthesis and characterization of poly(HEA/MALA) hydrogel and its application in removal of heavy metal ions from water, Chem. Eng. J. 215–216(15) (2013) 894–902.
[3] R.M. Shrestha, I. Varga, J. Bajtai, M. Varga, Design of surface functionalization of waste material originated charcoals by an optimized chemical carbonization for the purpose of heavy metal removal from industrial waste waters, Microchem. J. 108 (2013) 224–232.
[4] M. Kumar, H. Furumai, F. Kurisu, I. Kasuga, Potential mobility of heavy metals through coupled application of sequential extraction and isotopic exchange: Comparison of leaching tests applied to soil and soakaway sediment, Chemosphere 90(2) (2013) 796–804.
[5] D. Proust, C. Fontaine, N. Dauger, Impacts of weathering and clay mineralogy on heavy metals sorption in sludge-amended soils, CATENA 101 (2013) 188–196.
[6] K. Roy, D.K. Pal, S. Basu, D. Nayak, S. Lahiri, Synthesis of a new ion exchanger, zirconium vanadate, and its application to the separation of barium and cesium radionuclides at tracer levels, Appl. Radiat. Isot. 57 (2002) 471–474.

[7] G.M. Ibrahim, B. El-Gamma, I.M. El-Naggar, Synthesis and characterization of novel materials, tin potassium vanadate and zirconium potassium vanadate inorganic multi-component ion exchangers, Separ. Sci. Technol. 46 (2011) 664–678.
[8] A. Nilchi, M.R. Hadjmohammadi, S. Rasouli Garmarodi, R. Saberi, Studies on the adsorption behavior of trace amounts of $^{90}Sr^{2+}$, $^{140}La^{3+}$, $^{60}Co^{2+}$, $Ni^{2+}$and Zr^{4+} cations on synthesized inorganic ion exchangers, J. Hazard. Mater. 167 (2009) 531–535.
[9] E. Passaglia, R.A. Sheppard, The crystal chemistry of zeolites, Rev. Miner. Geochem. 45 (2001) 69–116.
[10] S. Merlino, M. Pasero, G. Artioli, A.P. Khomyakov, Penkvilksite, a new kind of silicate structure: OD character, X-ray single-crystal (1M), and powder Rietveld (2O) refinements of two MDO polytypes, Am. Mineral. 79 (1994) 1185–1193.
[11] G.D. Ilyushin, New data on the crystal structure of umbite K2ZrSi3O9*H2O, Izvestiya Akademii Nauk SSSR Neorganicheskie Materialy 29 (1993) 971–975.
[12] R.T. Downs, M. Hall-Wallace, The american mineralogist crystal structure database, Am. Mineral. 88 (2003) 247–250.
[13] Anonymous, Ion Exchange Chromatography & Chromatofocusing: Principles and Methods. Amersham Biosciences AB, Uppsala, 2004.
[14] N. Lendero, J. Vidic, P. Brne, V. Frankovic, A. Strancar, A. Podgornik, Characterization of ion exchange stationary phases via pH transition profiles, J. Chromatogr. A 1185 (2008) 59–70.
[15] J. Soto Pérez, D.D. Frey, Behavior of the inadvertent pH transient formed by a salt gradient in the ion-exchange chromatography of proteins, Biotechnol. Prog. 21(3) (2005) 902.
[16] T.M. Pabst, G. Carta, PH transitions in cation exchange chromatographic columns containing weak acid groups, J. Chromatogr. A 1142(1) (2007) 19–31.
[17] S. Ghose, T.M. McNerney, B. Hubbard, PH Transitions in ion-exchange systems: Role in the development of a cation-exchange process for a recombinant protein, Biotechnol. Prog. 18(3) (2002) 530.
[18] S.A. Nabi, Alimuddin, A.J. Islam, Synthesis and characterization of a new cation exchanger-zirconium(IV) iodotungstate: Separation and determination of metal ion contents of synthetic mixtures, pharmaceutical preparations and standard reference material, J. Hazard. Mater. 172 (2009) 202–207.
[19] W.A. Siddiqui, S.A. Khan, Synthesis, characterization and ion exchange properties of zirconium (IV) tungstoiodophosphate, a new cation exchanger, Bull. Mater. Sci. 30(1) (2007) 43–49.
[20] E.A. Hegazy, B. El-Gammal, F.H. Khalil, T.M. Mabrouk, Evaluation of anionic- and cationic-supported hydrogel membranes for sorption of Th(IV) and U(VI) Ions from nitric acid medium, J. Appl. Polym. Sci. 102 (2006) 320–332.
[21] B. El-Gammal, G.M. Ibrahim, K.F. Allan, I.M. El-Naggar, Modeling the PAAc-AN-TV surface using ^{134}Cs and $^{152+154}Eu$ sorption, J. Appl. Polym. Sci. 113(5) (2009) 3405–3416.
[22] I.A.W. Tan, A.L. Ahmad, B.H. Hameed, Adsorption of basic dye using activated carbon prepared from oil palm shell: batch and fixed bed studies, Desalination 225 (2008) 13–28.
[23] S.V. Mohan, N.C. Rao, J. Karthikeyan, Adsorptive removal of direct azo dye from aqueous phase onto coal based sorbents: A kinetic and mechanistic study, J. Hazard. Mater. 90 (2002) 189–204.